IEEE Access
Multidisciplinary | Rapid Review | Open Access Journal

Received 4 August 2022, accepted 3 September 2022, date of publication 8 September 2022, date of current version 22 September 2022.

Digital Object Identifier 10.1109/ACCESS.2022.3205324

RESEARCH ARTICLE

Influence of Eddy Current Loss on Electromagnetic Field and Temperature Field of High-Speed Permanent Magnet Generator With the Toroidal Windings

HONGBO QIU[1], ZHIHAO ZHU[1], BIN XIONG[2,3], AND CUNXIANG YANG[1]

[1]Electrical and Information Engineering Institute, Zhengzhou University of Light Industry, Zhengzhou 450002, China
[2]Institute of Electrical Engineering, Chinese Academy of Sciences, Beijing 100080, China
[3]University of Chinese Academy of Sciences, Beijing 100039, China

Corresponding author: Zhihao Zhu (zhu29777@163.com)

This work was supported in part by the National Natural Science Foundation of China under Grant U2004183 and Grant 52177063, in part by the Science and Technology Research Project of Science and Technology Department of Henan Province under Grant 202102210100, and in part by the Foundation for Key Teacher of Henan Province under Grant 2018GGJS087.

ABSTRACT The toroidal windings can shorten the axial length of the machine, so it is widely used in high-speed permanent magnet machine. However, under high-frequency operation, the magnetic flux leakage generated by the toroidal windings can cause a lot of eddy current loss on the shell, which will negatively influence the heat dissipation of the machine, resulting to overheating and the machine being unable to function. In this paper, the 40kW,20000rpm high-speed permanent magnet generator (HSPMG) with the toroidal windings is taken as an example to analysis the shell eddy current loss. Based on Laplace and Poisson equations, a quickly analytical calculation model of the shell eddy current loss is established, the influencing factors of the shell eddy current loss are elucidated. By using the finite element method (FEM), the influence of the shell structure and the shell material on the shell eddy current loss is studied, the mechanism of nonlinear variation of eddy current loss is revealed. In addition, the influence of load on the eddy current loss is studied. Furthermore, the 3-D temperature field calculation model of the generator is established, the influence of the shell eddy current loss on the generator temperature is studied, and the temperature distribution is obtained. Finally, the electromagnetic test and temperature rise experiment of the generator are carried out, while the experimental and finite element results are compared to verify the correctness of the model.

INDEX TERMS High-speed permanent magnet generator, analytical calculation, eddy current loss, 3-D temperature field, optimization design.

I. INTRODUCTION

In recent years, high-speed permanent magnet generator (HSPMG) has been widely used in gas turbines, distributed power generations and flywheels, because of its advantages of high efficiency, high power density and dynamic response capability [1], [2], [3]. The toroidal windings can shorten the axial length of the HSPMG, so the toroidal windings are frequently used in HSPMG, but the magnetic flux leakage generated by the toroidal windings can cause a lot of eddy current loss on the shell [4], [5], [6], [7], [8]. In addition, the shell is an important path of external heat dissipation, the shell eddy current loss has a negative impact on the overall heat dissipation of the generator. Since the HSPMG has high power density, its loss density is also large [9], [10], [11]. The generator overheating problem is serious that limits the growth in power density while also affecting the reliability of power supply [12], [13], [14].

The associate editor coordinating the review of this manuscript and approving it for publication was Xiaodong Liang.

TABLE 1. Comparative statements of reference papers.

Analytical Loss	Method	In this paper the problem is solved
Rotor and Shell	FEM[2-5]	A quickly analytical calculation model of loss is established
	Subdomain model[15-19]	
Structure optimization	Segmented structure[20][21]	The optimal shell structure is obtained.
	Low harmonic windings[23]	
Thermal influence	Temperature field[26-28]	Improve the temperature distribution of generator

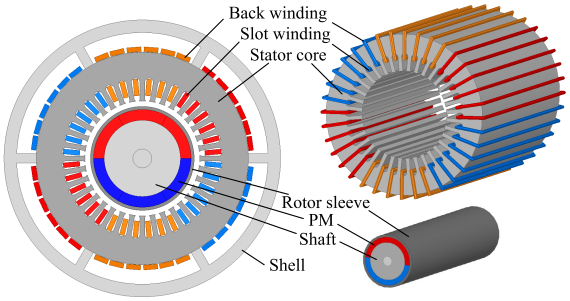

FIGURE 1. Structure of the HSPMG.

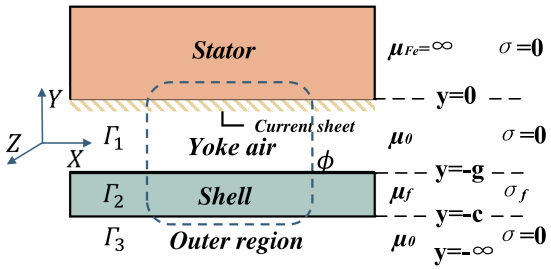

FIGURE 2. General-purpose model for shell eddy current loss calculation.

As for the HSPMG, the eddy current loss occupies a higher percentage of the total loss, so the eddy current loss is a key issue in the investigation. To improve the calculation accuracy, the subdomain model is proposed to calculate the PM loss [15], [16], [17], [18]. In [19], an improved rotor eddy current loss analysis model for PM machine is proposed, which the influences of time harmonics and space harmonics on the rotor eddy current loss are analyzed. Some researches concentrate on mitigating the rotor eddy current losses by the use of different rotor structures, including the segmented rotor, the surface slotted rotor, the segmented PM, and the axially segmented sleeve structure [20], [21]. In addition, there are some universal technologies that can be applied to mitigate the rotor eddy current losses in HSPMGs, such as rotor skewed slot and low harmonic stator windings [22], [23]. However, there is little research on the shell eddy current loss caused by magnetic flux leakage in toroidal windings. The shell can generate a lot of eddy current loss which is caused by the fundamental and harmonic magnetic motive force (MMF) generated by the back windings. The shell eddy current loss will influence the heat exchange of the HSPMGs [24], [25]. Overheating have directly affected the generators performance and even damages the generators [26], [27], [28]. Therefore, it is critical for HSPMGs to compute the shell eddy current loss and reduce the shell eddy current loss during the design stage. The comparative statements of reference papers are shown in Table 1.

In this article, aiming at the problem of high eddy current loss in HSPMG, the factors affecting the eddy current loss are studied. Based on Laplace and Poisson equations for calculating the shell eddy current loss for HSPMG with the toroidal windings, an analytical model has been proposed in Sections II. The factors affecting the eddy current loss are studied in Section III. In Section IV, the temperature distributions of these 3-D temperature models with various shells are compared. In Section V, one HSPMG with toroidal windings is manufactured and tested to validate the finite element results.

II. ANALYTICAL CALCULATION OF SHELL EDDY CURRENT LOSSES IN HSPMG

The toroidal windings, which have one side immersed in the stator core groove and the other side on the back of the stator yoke, can effectively shorten the length of the end of the stator winding and thus greatly reduce the length of the rotor, thus ensuring the mechanical strength of the HSPMG. The structure of HSPMG with the toroidal windings is shown in Fig. 1.

The solution region of model is divided into four regions: the stator, the yoke air, the shell and the outer region according to the structure of the HSPMG. To derive an analytical solution of the shell eddy current loss, the following assumptions are made:

1) The MMF of the toroidal windings located between the stator and the shell is equivalent to the current sheet.

2) The permeability of the stator core is infinite.

3) Approximating that the stator and the shell are flat surface.

4) The saturation and hysteresis effects of the core are ignored.

For the HSPMG, the flux distribution variation along the axial is small in the machine and the magnetic field could be considered as a series of parallel plane field perpendicular to the axial direction. The calculation of the shell eddy currents loss is simplified to a two-dimensional electromagnetic field. In this article, the model used for the analytical derivation of the shell of HSPMG with the toroidal windings is shown in Fig. 2.

The current is sinusoidal distribution in both space and time which can be described by the expression:

$$J_0 = k_z J_{0m} \cos\left(\omega t - \frac{\pi}{\tau}x\right) = k_z Re\left[J_{0m} e^{i\left(\omega - \frac{\pi}{\tau}x\right)}\right] \quad (1)$$

$$J_{0m} = \frac{3\sqrt{2}N_1 k_{w1} I}{p_0 \tau} \quad (2)$$

where J_0 is the electrical load, k_z is the unit vector of z-axis direction, J_{0m} is the amplitude of electrical load, generated by the symmetrical three-phase current in the toroidal windings, N_1 is the number of turns per phase, k_{w1} is the fundamental windings factor, p_0 is the number of pole pairs, and τ is the pole pitch and I is the RMS value of the phase current.

Due to electrical load J_{0m} in the z-direction, the vector magnetic potentials in each region are z-directional.

$$\begin{aligned} A(x,y,t) &= k_z A_z \qquad (3)\\ A_z &= A_z(y)\cos\left(\omega t - \frac{\pi}{\tau}x - \varphi\right)\\ &= Re\left[\dot{A}_z e^{j(\omega t - \frac{\pi}{\tau}x)}\right] \qquad (4)\end{aligned}$$

Based on the analytical calculation model, the vector magnetic potential equations for each region are determined:

$$\begin{cases} \nabla^2\dot{A}_{za} = 0 \ (-g \le y \le 0)\\ \nabla^2\dot{A}_{zf} - j\omega_v\mu_f\sigma_f\dot{A}_{zf} = 0 \ (-c \le y \le -g)\\ \nabla^2\dot{A}_{zz} = 0 \ (y \le -c) \end{cases} \qquad (5)$$

$$\begin{cases} \dfrac{\partial^2\dot{A}_{za}}{\partial x^2} + \dfrac{\partial^2\dot{A}_{za}}{\partial y^2} = 0 \ (-g \le y \le 0)\\ \dfrac{\partial^2\dot{A}_{zf}}{\partial x^2} + \dfrac{\partial^2\dot{A}_{zf}}{\partial y^2} = j\omega_v\mu_f\sigma_f\dot{A}_{zf} \ (-c \le y \le -g)\\ 7pt]\dfrac{\partial^2\dot{A}_{zz}}{\partial x^2} + \dfrac{\partial^2\dot{A}_{zz}}{\partial y^2} = 0 \ (y \le -c) \end{cases} \qquad (6)$$

where $\dot{A}_{za}$, $\dot{A}_{zf}$ and $\dot{A}_{zz}$ are the vector magnetic potentials of the yoke air region, the shell region and the outer region respectively, μ_f is the magnetic permeability of the shell region, σ_f is the electrical conductivity of the shell region.

Considering the sinusoidal electromagnetic field at steady-state $\frac{\partial}{\partial t} = j\omega_v$, $\frac{\partial}{\partial x} = -j\frac{\pi}{\tau_v}$, then $\frac{\partial^2\dot{A}_{za}}{\partial x^2} = \left(-j\frac{\pi}{\tau_v}\right)^2\dot{A}_{za}$, where ω_v and τ_v are changed with harmonic order v. The above set of equations is simplified to be obtained as:

$$\begin{cases} \Gamma_1 : \dfrac{\partial^2\dot{A}_{za}}{\partial y^2} - \left(\dfrac{\pi}{\tau_v}\right)^2\dot{A}_{za} = 0\\ \Gamma_2 : \dfrac{\partial^2\dot{A}_{zf}}{\partial y^2} - \left[\left(\dfrac{\pi}{\tau_v}\right)^2 + j\omega_v\mu_f\sigma_f\right]\dot{A}_{zf} = 0\\ \Gamma_3 : \dfrac{\partial^2\dot{A}_{zz}}{\partial x^2} + \dfrac{\partial^2\dot{A}_{zz}}{\partial y^2} = 0 \end{cases} \qquad (7)$$

The magnetic potential vector for each region can be obtained, and the magnetic potential vector for each region is

$$\begin{cases} \dot{A}_{za} = c_1^a sh\dfrac{\pi}{\tau_v}y + c_2^a ch\dfrac{\pi}{\tau_v}y\\ \dot{A}_{zf} = c_1^f sh\beta y + c_2^f ch\beta y\\ \dot{A}_{zz} = c_1^z e^{\frac{\pi}{\tau_v}y} + c_2^z e^{-\frac{\pi}{\tau_v}y} \end{cases} \qquad (8)$$

where the coefficients c_1^a, c_2^a, c_1^f, c_2^f, c_1^z and c_2^z can be determined by the boundary conditions.

A. The permeability of the stator core is infinite, so the magnetic field intensity in stator core is 0A/m. The tangential component of the magnetic field intensity on the surface of the stator core is equal to the value of electric load, and the boundary condition between the stator yoke and the yoke air can be obtained as:

$$\dot{H}_{xa}\big|_{y=0} = \frac{1}{\mu_0}\frac{\partial\dot{A}_{za}}{\partial y} = J_{0m} \qquad (9)$$

where J_{0m} is the current sheet amplitude. Since $c_1^a = \mu_0\frac{\tau_v}{\pi}J_{0m}$, this means that:

$$\dot{A}_{za} = \mu_0\frac{\tau_v}{\pi}J_{0m}sh\frac{\pi}{\tau_v}y + c_2^a ch\frac{\pi}{\tau_v}y \qquad (10)$$

B. At the boundary between the yoke air region and the shell region, the magnetic flux density is continuous in the normal direction, the magnetic field intensity is continuous in the tangential direction. The boundary condition between the yoke air region and the shell is

$$\begin{cases} B_n|_{y=-g} = -\left.\dfrac{\partial\dot{A}_{za}}{\partial x}\right|_{y=-g} = -\left.\dfrac{\partial\dot{A}_{zf}}{\partial x}\right|_{y=-g}\\ H_t|_{y=-g} = \left.\dfrac{1}{\mu_0}\dfrac{\partial\dot{A}_{za}}{\partial y}\right|_{y=-g} = \left.\dfrac{1}{\mu_f}\dfrac{\partial\dot{A}_{zf}}{\partial y}\right|_{y=-g} \end{cases} \qquad (11)$$

Since $\frac{\partial}{\partial x} = -j\frac{\pi}{\tau_v}$, this means that:

$$\dot{A}_{za}\big|_{y=-g} = \dot{A}_{zf}\big|_{y=-g} \qquad (12)$$

C. The boundary condition between the shell and the outer region is

$$\dot{A}_{zf}\big|_{y=-c} = \dot{A}_{zz}\big|_{y=-c} \qquad (13)$$

$$H_t|_{y=-c} = \left.\frac{1}{\mu_f}\frac{\partial\dot{A}_{zf}}{\partial y}\right|_{y=-c} = \left.\frac{1}{\mu_0}\frac{\partial\dot{A}_{zz}}{\partial y}\right|_{y=-c} \qquad (14)$$

D. When y tends to infinity of the negative plane in the outside shell region,$\dot{A}_{zz}$ is finite and thus $c_2^z = 0$, this means that:

$$\dot{A}_{zz} = c_1^z e^{\frac{\pi}{\tau_v}y} \qquad (15)$$

Based on the magnetic vector equations and boundary conditions for each region, the group of equations can be listed as follows:

$$\begin{cases} -\mu_0\dfrac{\tau_v}{\pi}J_{0m}sh\dfrac{\pi}{\tau_v}g + c_2^a ch\dfrac{\pi}{\tau_v}g = -c_1^f sh\beta g + c_2^f ch\beta g\\ \dfrac{1}{\mu_0}\left(\mu_0 J_{0m}ch\dfrac{\pi}{\tau_v}g - c_2^a\dfrac{\pi}{\tau_v}g\right) = \dfrac{1}{\mu_f}c_1^f\beta ch\beta g - \dfrac{1}{\mu_f}c_2^f\beta sh\beta g\\ -c_1^f sh\beta c + c_2^f ch\beta c = c_1^z e^{-\frac{\pi}{\tau_v}c}\\ \dfrac{1}{\mu_f}\left(c_1^f\beta ch\beta c - c_2^f\beta sh\beta c\right) = \dfrac{1}{\mu_0}c_1^z\dfrac{\pi}{\tau_v}e^{-\frac{x}{\tau_v}c} \end{cases} \qquad (16)$$

It can be seen that the unique solution can be obtained by solving the set of equations shown in

(16). These equations can be represented in matrix form as (17):

$$Ax = B \tag{17}$$

$$A = \begin{bmatrix} ch\frac{\pi}{\tau_v}g & sh\beta g & -ch\beta g & 0 \\ -\frac{1}{\mu_0}\frac{\pi}{\tau_v}g & -\frac{1}{\mu_f}\beta ch\beta g & \frac{1}{\mu_f}\beta sh\beta g & 0 \\ 0 & -sh\beta c & ch\beta c & -e^{-\frac{x}{\tau_v}c} \\ 0 & \frac{1}{\mu_f}\beta ch\beta c & -\frac{1}{\mu_f}\beta sh\beta c & -\frac{1}{\mu_0}\frac{\pi}{\tau_v}e^{-\frac{x}{\tau_v}c} \end{bmatrix} \tag{18}$$

$$B = \left[\mu_0\frac{\tau_v}{\pi}J_{0m}sh\frac{\pi}{\tau_v}g; -\frac{1}{\mu_0}\mu_0 J_{0m}ch\frac{\pi}{\tau_v}g; 0; 0\right] \tag{19}$$

$$x = \left[c_2^a, c_1^f, c_2^f, c_1^z\right] \tag{20}$$

By solving the above matrix, the coefficient in the vector magnetic potentials of each region can be determined. The expression for the eddy current in the shell of the HSPMG is

$$\dot{J}_{zf} = -j\omega_v\sigma_f\dot{A}_{zf} = -j\omega_v\sigma_f\left(c_1^f sh\beta y + c_2^f ch\beta y\right) \tag{21}$$

The eddy current loss in the solid conductors is determined from the joule loss:

$$P_f = \frac{1}{2}Lh\int_g^c \frac{\left|\dot{J}_{zf}\right|^2}{\sigma_f}dy \tag{22}$$

where L is the equivalent length of the circumference of the shell in Cartesian coordinates, h is the axial length of the HSPMG.

According to the formula (22), the shell eddy current loss is affected by the value and distribution of eddy current density on the shell. The eddy current density is closely related to the vector magnetic potential in the region of eddy current, and the vector magnetic potential in the eddy current region is affected by the equivalent boundary condition of the MMF and the size of the model, so there are complex factors affecting the eddy current loss. In order to verify the accuracy of the analytical formula, the FEM (Ansys) is used for detailed analysis below.

III. FEM MODEL ESTABLISH AND ANALYZE

In this paper, the 40kW, 20,000rpm HSPMG with the toroidal windings is taken as an example. The basic parameters of the HSPMG are shown in Table 2. The field-circuit coupling method is used to study the shell eddy current loss of the HSPMG, using a 2-D transient electromagnetic model. Fig. 3 shows the winding connection of HSPMG.

The finite element model is shown in Fig. 4. At high frequency, the skin effect will be considered. In order to accurately calculate the shell eddy current loss, the number of elements in the model subdivision of shell is increased.

A. INFLUENCE OF THE SHELL STRUCTURE ON THE SHELL EDDY CURRENT LOSS

Fig. 5 shows the variation in eddy current loss at various HSPMG rotational speeds, the eddy current loss increases with the operating frequency. When the HSPMG is operating at 20,000r/min, the shell eddy current loss, the PM eddy current loss and the rotor sleeve eddy current loss is 70.3W, 13.4W and 9.2W. For the HSPMG with the toroidal windings, the eddy current is mainly concentrated on the rotor and the shell. The shell is influenced by the fundamental and harmonic MMF generated by the toroidal windings due to the fixed structure that the shell is relatively stationary to the

TABLE 2. The parameters of the HSPMG.

Basic parameters	Value
Rated power (kW)	40
Number of turns per slot	5
Pole number	2
Rotor type	PM(NdFe35)
Frequency (Hz)	333.33
Slot number	36
Stator outer diameter (mm)	135
Stator inner diameter (mm)	72
Rotor outer diameter (mm)	66
Shell outer diameter (mm)	168
Shell inner diameter (mm)	160
Shell materials	aluminium
Conductivity of shell (S/m)	3.8E7
Permeability of shell (u0)	1

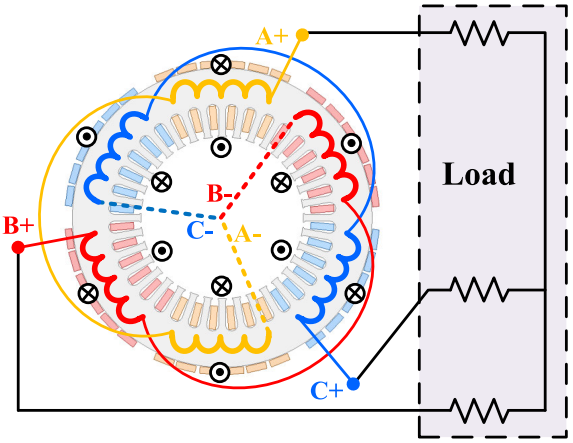

FIGURE 3. The winding connection of HSPMG.

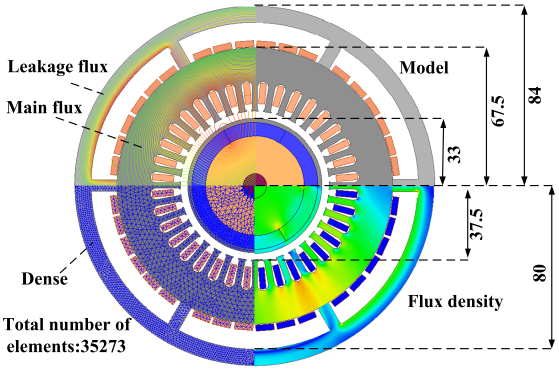

FIGURE 4. Finite element model.

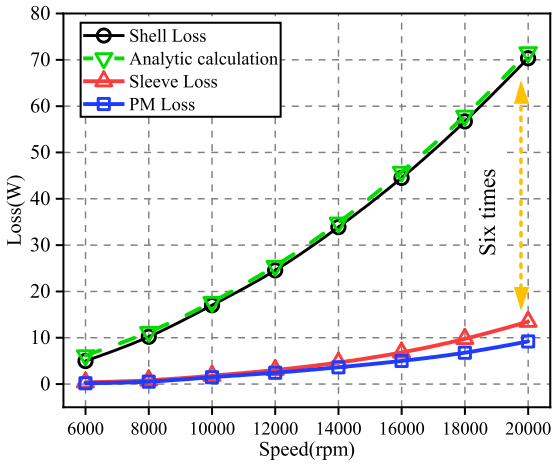

FIGURE 5. The eddy current losses of the generator with different speed.

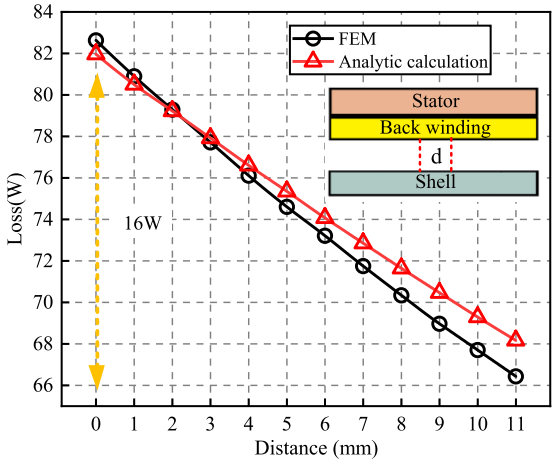

FIGURE 6. The shell eddy current losses of different distance(d).

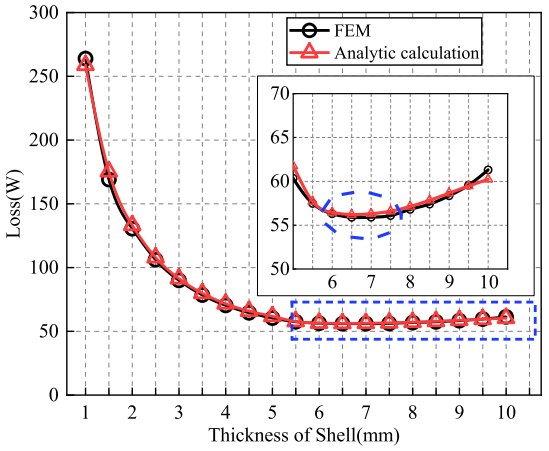

FIGURE 7. The shell eddy current losses with different thicknesses shell.

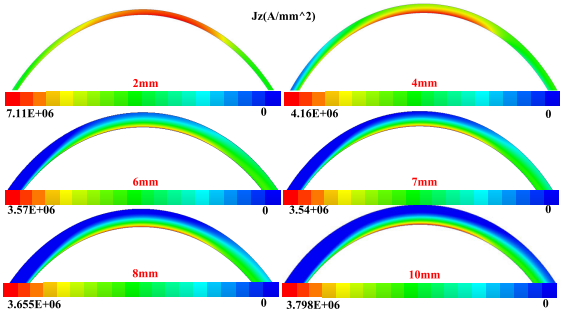

FIGURE 8. The eddy current density distribution of the shell with different thicknesses shell.

stator. So the shell loss is greater than the PM loss and the sleeve loss. In addition, comparing the results of FEM and the analytical method, both results are in good agreement.

The variation of the shell eddy current loss with the distance (d) between the shell and the back windings is shown in Fig. 6. When the distance increases from 0mm to 11mm, the magnetic resistance of the yoke air region is increased. The influence of the magnetic flux leakage on the shell loss is reduced, so the shell eddy current loss decreases from 82.6W to 66.4W.

According to the formula (22), the eddy current loss is also affected by the shell thickness. As can be seen from Fig. 7, when the shell thickness is increased from 1mm to 3mm, the shell eddy current loss drops dramatically from 263.9W to 89.8W. When the shell thickness is increased from 3mm to 10mm, the loss first decreases and then increases slightly with a minimum of 55.9W at 7mm.

By using the FEM, the influence of the value and distribution of current density on the shell eddy current loss is determined. As shown in Fig. 8, since the eddy current distribution is affected by skin effect, the eddy current is mainly distributed on the inner surface of the shell. When the shell thickness is 2mm, the maximum current density of the shell is 7.11×6 A/m2. Therefore, the shell eddy current loss with a thickness of 2mm is large. When the shell thickness is 6mm, 7mm, 8mm and 10mm, the current density is observable decreased, and the current density is the smallest at the thickness of 7mm, so the shell eddy current loss is the smallest.

It has been determined that a shell with too thin thickness will result in the significant increase of the shell eddy current loss, and a thick shell leads to the slight increase of the loss. Therefore, the optimal shell thickness has the minimization of the shell eddy current loss, improving the heat dissipation of the generator.

Metal is commonly used as the shell material. The FEM is used to study the effect of different materials on the shell eddy current loss, and the calculated results are shown in Fig. 9.

As shown in Fig. 9, the loss in the shell with high conductivity and low permeability material is little. While the loss in the shell with low conductivity and high permeability material is great. When the loss is 70W, the material has the conductivity of 3.8E+7 (S/m) and permeability of 1 (μ_0). When the loss is 2080W, the material has the conductivity of 2.0E+6 (S/m) and permeability of 1000 (μ_0). When

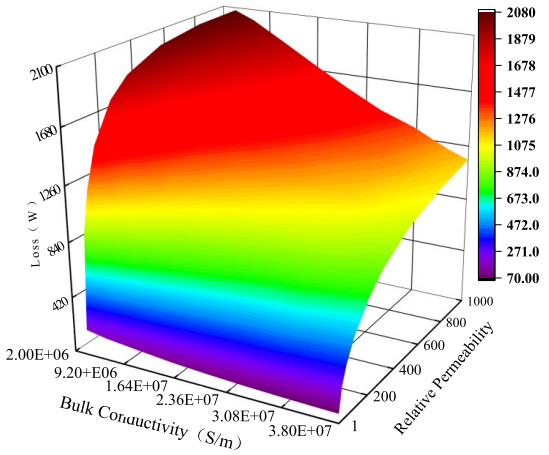

FIGURE 9. The shell eddy current loss of different materials.

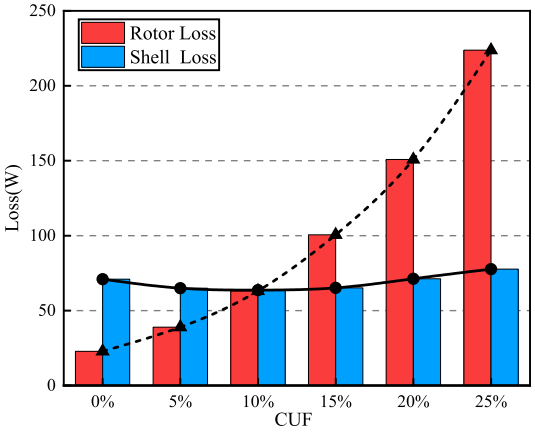

FIGURE 10. The eddy current losses of the generator under different CUFs.

TABLE 3. The shell eddy current loss.

Harmonic order	1	5	7	11
Loss for analytic calculation (W)	76.7	28.4	4.3	1.1
Total loss for analytic calculation (W)		110.7		
Total loss for FEM (W)		105.4		

the shell material is aluminum, cast iron, low carbon steel, stainless steel, and aluminum alloy, the corresponding shell eddy current losses are 70W, 1430W, 2080W, 258W, and 295W, respectively. Therefore, the shell should be made of the material with high conductivity and low permeability, which can reduce the eddy current loss.

B. INFLUENCE OF DIFFERENT LOAD CONDITIONS ON THE SHELL EDDY CURRENT LOSS

HSMPG is a importance equipment in distributed energy supply system. When the load fluctuation or fault occurred, the current unbalance would appear in the generator stator windings. The performance of generator will be influenced by the unbalance current.

In order to measure the unbalance degree of generator load, the current unbalance coefficient (CUF) is adopted as the measuring standard. The calculation formula of CUF is shown in (23).

$$CUF = \frac{MAX\left[\left|I_a - I_{avg}\right| \left|I_b - I_{avg}\right| \left|I_c - I_{avg}\right|\right]}{I_{avg}} \quad (23)$$

where I_a, I_b, and I_c are the RMS of the three-phase current and I_{avg} is the average of I_a, I_b, and I_c.

In this section, the output power of the generator is the rated power. The influences of different CUFs (0%, 5%, 10%, 15%,20%, and 25%) on the eddy current losses of the generator are studied quantitatively.

The eddy current losses are shown in Fig. 10, it can be seen that with the increase of the unbalance rate, the shell eddy current loss does not change, but the rotor eddy current loss increases. When CUF is 25%, the rotor eddy current loss is 223.8 W, which is ten times of that when CUF is 0%. Therefore, the current unbalance has no effect on the shell eddy current loss, but has a significant effect on the rotor eddy current loss.

A power converter is very necessary in the system of HSPMG, since the frequency of the output electrical energy is generally hundreds of Hertz. However, the converter is a nonlinear load, which generates a large number of harmonic components in the generator, the harmonic will affect the performance of the generator. Therefore, the shell eddy current loss of generator with the rated power is analyzed by combining Fourier theory. The current sheet equation is calculated for time and space harmonic MMF and the total losses are calculated by summing the harmonic loss. The harmonic losses are shown in Table 3.

It can be seen that the shell eddy current loss increases under the condition of the nonlinear load, which is 49.9% higher than that under the condition of linear load. The loss caused by the fundamental magnetic field accounts for 69.4% of the total loss, and the loss caused by the fifth harmonic magnetic field accounts for 25.7% of the total loss. The results show that the fundamental magnetic field and the fifth harmonic magnetic field are the main factors affecting the shell eddy current loss.

IV. 3-D TEMPERATURE FIELD MODEL ESTABLISH AND ANALYZE

HSPMG is small size and high power density, so the temperature rise of HSPMG is higher than the traditional machinery. Excessive temperature will affect the reliability of the generator. Therefore, it is important for the generator operating at the safe temperature. The generator adopts the closed oil cooling method, and the schematic diagram of the cooling system is shown in Fig.11. The cooling medium flows through the stator slot and yoke back room along the axial direction, by which stator windings and core are directly cooled. There is an oil separator (epoxy resin board) in the air gap adjacent

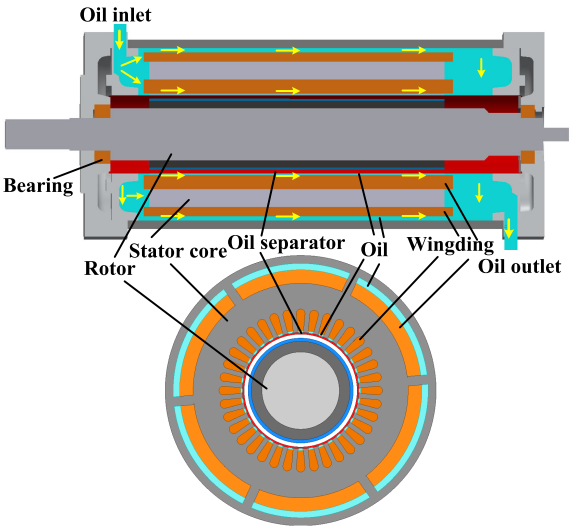

FIGURE 11. Cooling system of the generator.

TABLE 4. Values of heat source and thermal parameters of the main components.

Components	Materials	Loss(W)	Thermal conductivity (W/(m·K))
Aluminum shell	Aluminum	70.3	202.4
Steel shell	Cast iron	1430.1	35
Stator core	Silicon lamination	837.9	4.5, 42.5
Winding	Copper	170.9	387.6
Sleeve	Austenite	13.4	12.2
PM	NdFe35	9.2	8
Insulation	Epoxy resin board	0	0.015
Cooling medium	Oil	0	0.12974

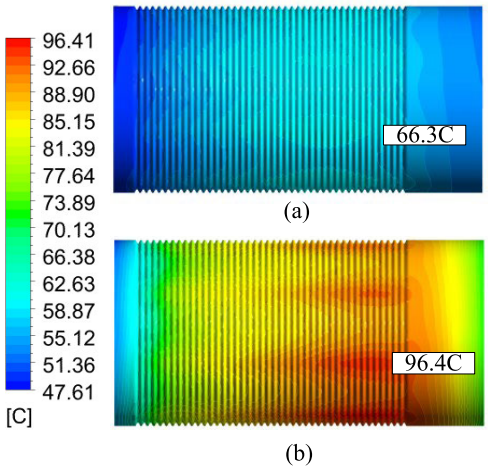

FIGURE 12. Temperature distribution of the shell (a) aluminum shell (b) steel shell.

to the stator core inner surface and end closures to ensure that the oil cooling system is completely closed in the stator side.

Based on the analysis in Sections II and III, the loss of each part are obtained, as shown in Table 4. The oil flow rate is 5L/min, and the inlet temperature is 38°C.

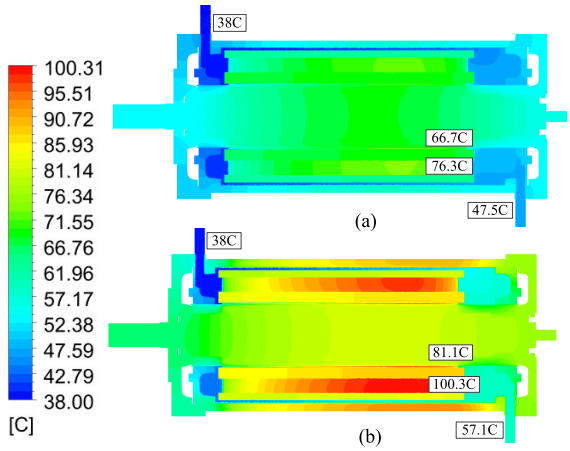

FIGURE 13. Temperature distribution of the generator (a) aluminum shell (b) steel shell.

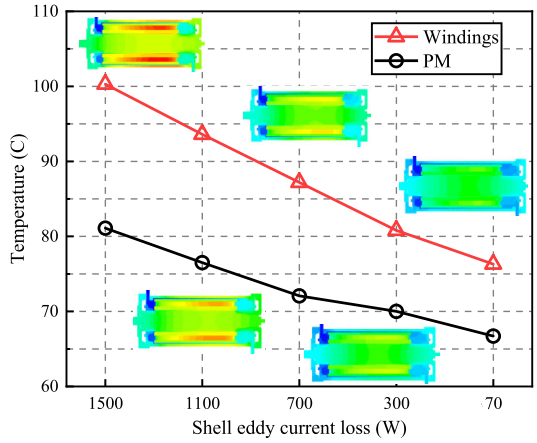

FIGURE 14. Temperature with the different of the shell eddy current loss.

Fig.12. shows the temperature distribution of the aluminum and steel shell. The highest temperature of the aluminum shell is 66.3°C, the steel shell temperature reaches 96.4°C.

Due to the different temperatures of the aluminum shell and the steel shell, the influences on the heat exchange of the generator is also different. Fig. 13 shows the temperature distribution of the two generators. It is clear that the generator of the steel shell has a higher temperature than the generator of the aluminum shell. The maximum temperature at the windings of the two generators is 76.3 °C for aluminum shell generator and 100.3 °C for steel shell generator, with a difference of 24 °C. The PM temperature of the aluminum shell generator is 66.7°C, while the PM temperature of the steel shell generator is 81.1°C, with a difference of 14.4°C. The overall temperature of the generator with the steel shell is 20.2% higher than that of the generator with the aluminum shell. This is due to the high temperature of the steel shell, which negatively affects the heat dissipation of generator.

Fig. 14 shows the PM temperature and windings temperature with the different of the shell eddy current loss. With the

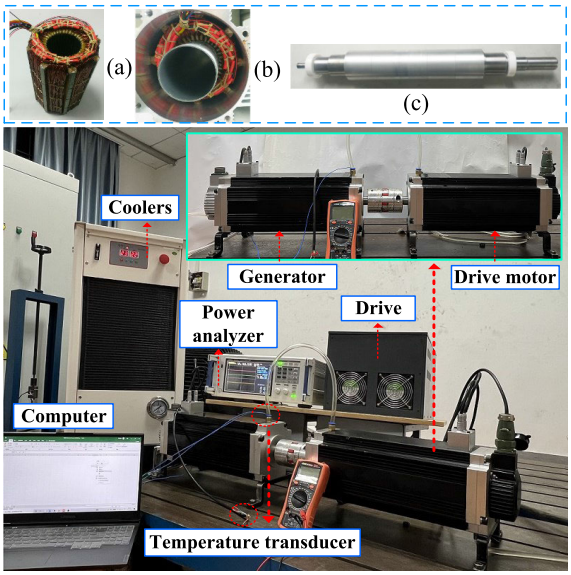

FIGURE 15. Test rig for the measurement of HSPMG.(a) Stator with toroidal windings. (b) Stator assembly. (c) Rotor.

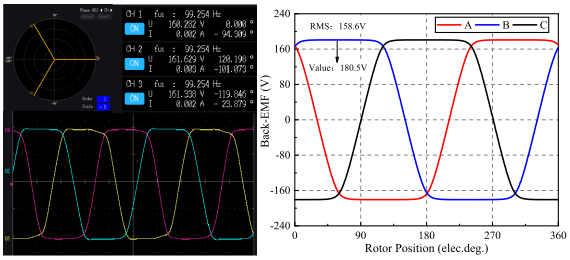

FIGURE 16. Comparison of no-load back-EMF waveforms. (a) Experimental test waveforms. (b) FEM waveforms.

decrease of the shell eddy current loss, the PM and windings temperature is also reduced.

The above analysis shows that the overheating of the shell has an adverse effect on the heat dissipation of the generator. Therefore, reducing the shell eddy current loss can effectively reduce the temperature of the generator, which is beneficial to the operation of the generator.

V. EXPERIMENTAL VALIDATION

In this section, a HSPMG is manufactured and tested. Fig. 15 shows a test rig for the measurement. The no-load back-EMF of the prototype is measured, which is shown in Fig. 16. It can be seen that the RMS of the 6000 rpm no-load back-EMF of the experimental test (161.3 V) agrees well with that of the FEM (158.6 V), with an error of 1.7%.

During the experimental of temperature field, the oil flow rate is kept as 1.8 L/min. The temperature rise of the generator is stable after 140 minutes. Meanwhile, temperatures at HSPMG different positions are also measured.

The temperature rise experiment of the prototype is carried out, and the results are shown in Fig. 17. The temperature

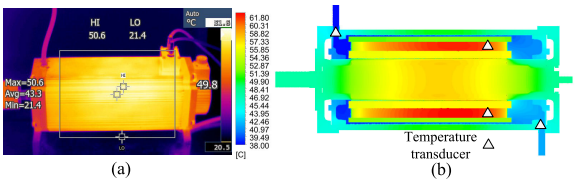

FIGURE 17. Temperature distribution of the generator. (a) Measurement. (b) simulation.

of prototype winding is 57.3°C, while the temperature of 3-D model winding is 60.3°C. The temperature of prototype shell is 49.8°C, while the temperature of 3-D model shell is 52.8°C with an error of 6%, which validates the feasibility of the proposed machine and the correctness of the analysis mentioned above.

VI. CONCLUSION

In this paper, the 40kW, 20,000rpm HSPMG with the toroidal windings is taken as an example. The additional loss of shell is studied by analytical calculation method and FEM. The research conclusions are as follows:

1) An accurate analytical method for calculating the shell eddy current loss is proposed. The analytical formula can quick calculate the loss, which reduces the calculation time compared with the FEM. The influence of the shell structure and the shell material on the shell eddy current loss is confirmed, the nonlinear variation mechanism of shell thickness on loss is revealed. The optimal shell thickness with minimum shell eddy current loss is obtained.

2) The eddy current loss will be increased by the current unbalance. When CUF is 25%, the rotor eddy current loss is 223.8 W, which is ten times of that when CUF is 0%. But the shell eddy current loss is unchanged. Therefore, the current unbalance has no effect on the shell eddy current loss.

3) The shell eddy current loss increases under the condition of the nonlinear load, which is 49.9% higher than that under the condition of linear load. The loss caused by the fundamental magnetic field accounts for 69.4% of the total loss, and the loss caused by the fifth harmonic magnetic field accounts for 25.7% of the total loss. The fundamental magnetic field and the fifth harmonic magnetic field are the main factors affecting the shell eddy current losses.

4) The eddy current loss of shell has a great influence on the heat dissipation of the HSPMG. The overall temperature of the generator with the steel shell is 20.2% higher than that of the generator with the aluminum shell. Therefore, reducing the eddy current loss can obvious improve the temperature distribution of the generator.

REFERENCES

[1] N. Uzhegov, A. Smirnov, C. H. Park, J. H. Ahn, J. Heikkinen, and J. Pyrhönen, "Design aspects of high-speed electrical machines with active magnetic bearings for compressor applications," *IEEE Trans. Ind. Electron.*, vol. 64, no. 11, pp. 8427–8436, Nov. 2017.

[2] F. Xu, T. He, Z. Q. Zhu, Y. Wang, S. Cai, H. Bin, D. Wu, L. Gong, and J. Chen, "Influence of slot number on electromagnetic performance of 2-pole high-speed permanent magnet motors with toroidal windings," *IEEE Trans. Ind. Appl.*, vol. 57, no. 6, pp. 6023–6033, Nov. 2021.

[3] C. Gong, S. Li, and T. Habetler, "High-strength rotor design for ultra-high speed switched reluctance machines," *IEEE Trans. Ind. Appl.*, vol. 56, no. 2, pp. 1432–1442, Mar. 2020.
[4] H. Li, Z. Q. Zhu, and H. Hua, "Comparative analysis of flux reversal permanent magnet machines with toroidal and concentrated windings," *IEEE Trans. Ind. Electron.*, vol. 67, no. 7, pp. 5278–5290, Jul. 2020.
[5] D. Li, R. Qu, J. Li, and W. Xu, "Consequent-pole toroidal-winding outer-rotor Vernier permanent-magnet machines," *IEEE Trans. Ind. Appl.*, vol. 51, no. 6, pp. 4470–4481, Nov./Dec. 2015.
[6] Z. Jia, H. Lin, S. Fang, and Y. Huang, "A novel transverse flux permanent magnet generator with double C-Hoop stator and flux-concentrated rotor," *IEEE Trans. Magn.*, vol. 51, no. 11, pp. 1–4, Nov. 2015.
[7] X. Wang, M. Zhao, Y. Zhou, Z. Wan, and W. Xu, "Design and analysis for multi-disc coreless axial-flux permanent-magnet synchronous machine," *IEEE Trans. Appl. Supercond.*, vol. 31, no. 8, pp. 1–4, Nov. 2021.
[8] X. Liu, G. Liu, and B. Han, "A loss separation method of a high-speed magnetic levitated PMSM based on drag system experiment without torque meter," *IEEE Trans. Ind. Electron.*, vol. 66, no. 4, pp. 2976–2986, Apr. 2019.
[9] G. Du, Q. Zhou, S. Liu, N. Huang, and X. Chen, "Multiphysics design and multiobjective optimization for high-speed permanent magnet machines," *IEEE Trans. Transport. Electrific.*, vol. 6, no. 3, pp. 1084–1092, Sep. 2020.
[10] D. Gerada, A. Mebarki, N. L. Brown, K. J. Bradley, and C. Gerada, "Design aspects of high-speed high-power-density laminated-rotor induction machines," *IEEE Trans. Ind. Appl.*, vol. 58, no. 9, pp. 4039–4047, Sep. 2011.
[11] M. van der Geest, H. Polinder, J. A. Ferreira, and M. Christmann, "Power density limits and design trends of high-speed permanent magnet synchronous machines," *IEEE Trans. Transport. Electrific.*, vol. 1, no. 3, pp. 266–276, Oct. 2015.
[12] C. Carounagarane, T. R. Chelliah, and D. Khare, "Analysis on thermal behavior of large hydrogenerators operating with continuous overloads," *IEEE Trans. Ind. Appl.*, vol. 56, no. 2, pp. 1293–1305, Mar. 2020.
[13] H. Jichao, S. Yutian, Z. Ping, Q. Haiming, D. Jiechen, L. Yufei, Z. Chunli, G. Baojun, and L. Weili, "Influence of complex fluid flow on temperature distribution in the rotor region of large hydrogenerator under the rotor rotation," *IEEE Access*, vol. 10, pp. 3252–3262, 2022.
[14] H. Jichao, L. Yufei, D. Jiechen, S. Yutian, G. Baojun, and L. Weili, "Thermal modeling and experimental validation in the rotor region of hydrogenerator with different rotor structures," *IEEE Access*, vol. 9, pp. 120001–120009, 2021.
[15] S.-M. Jang, H.-W. Cho, S.-H. Lee, H.-S. Yang, and Y.-H. Jeong, "The influence of magnetization pattern on the rotor losses of permanent magnet high-speed machines," *IEEE Trans. Magn.*, vol. 40, no. 4, pp. 2062–2064, Jul. 2004.
[16] L. J. Wu, Z. Q. Zhu, D. Staton, M. Popescu, and D. Hawkins, "An improved subdomain model for predicting magnetic field of surface-mounted permanent magnet machines accounting for tooth-tips," *IEEE Trans. Magn.*, vol. 47, no. 6, pp. 1693–1704, Jun. 2011.
[17] H. Toda, Z. Xia, J. Wang, K. Atallah, and D. Howe, "Rotor eddy-current loss in permanent magnet brushless machines," *IEEE Trans. Magn.*, vol. 40, no. 4, pp. 2104–2106, Jul. 2004.
[18] Z. Zhang, Z. Deng, Q. Sun, C. Peng, Y. Gu, and G. Pang, "Analytical modeling and experimental validation of rotor harmonic eddy-current loss in high-speed surface-mounted permanent magnet motors," *IEEE Trans. Magn.*, vol. 55, no. 2, pp. 1–11, Feb. 2019.
[19] N. Chiodetto, N. Bianchi, and L. Alberti, "Improved analytical estimation of rotor losses in high-speed surface-mounted PM synchronous machines," *IEEE Trans. Ind. Appl.*, vol. 53, no. 4, pp. 3548–3556, Jul. 2017.
[20] J.-X. Shen, H. Hao, M.-J. Jin, and C. Yuan, "Reduction of rotor eddy current loss in high speed PM brushless machines by grooving retaining sleeve," *IEEE Trans. Magn.*, vol. 49, no. 7, pp. 3973–3976, Jul. 2013.
[21] H.-W. Jun, J. Lee, H.-W. Lee, and W.-H. Kim, "Study on the optimal rotor retaining sleeve structure for the reduction of eddy-current loss in high-speed SPMSM," *IEEE Trans. Magn.*, vol. 51, no. 3, pp. 1–4, Mar. 2015.
[22] P. Lazari, J. Wang, and B. Sen, "3-D effects of rotor step-skews in permanent magnet-assisted synchronous reluctance machines," *IEEE Trans. Magn.*, vol. 51, no. 11, pp. 1–4, Nov. 2015.
[23] O. Misir, S. M. Raziee, N. Hammouche, C. Klaus, R. Kluge, and B. Ponick, "Prediction of losses and efficiency for three-phase induction machines equipped with combined star-delta windings," *IEEE Trans. Ind. Appl.*, vol. 53, no. 4, pp. 3579–3587, Jul./Aug. 2017.
[24] M.-K. Seo, Y.-Y. Ko, T.-Y. Lee, Y.-J. Kim, and S.-Y. Jung, "Loss reduction optimization for heat capacity improvement in interior permanent magnet synchronous machine," *IEEE Trans. Magn.*, vol. 54, no. 11, pp. 1–5, Nov. 2018.
[25] J. Nerg, M. Rilla, and J. Pyrhönen, "Thermal analysis of radial-flux electrical machines with a high power density," *IEEE Trans. Ind. Electron.*, vol. 55, no. 10, pp. 3543–3554, Oct. 2008.
[26] Z. Huang, J. Fang, X. Liu, and B. Han, "Loss calculation and thermal analysis of rotors supported by active magnetic bearings for high-speed permanent-magnet electrical machines," *IEEE Trans. Ind. Electron.*, vol. 63, no. 4, pp. 2027–2035, Apr. 2016.
[27] Y. Xu, N. Maki, and M. Izumi, "Operating temperature influence on performance of 10 MW wind turbine HTS generators," *IEEE Trans. Appl. Supercond.*, vol. 25, no. 3, pp. 1–5, Jun. 2015.
[28] W. Liu, W. Li, S. Luo, X. Huang, D. Li, Z. Li, and G. Xu, "Influence of a novel stator teeth internal ventilation structure on air-cooled turbo-generator parameters and stator temperature," *IEEE Access*, vol. 8, pp. 122422–122433, 2020.

HONGBO QIU received the graduate degree from the Harbin University of Science and Technology, Harbin, China, where he received the Ph.D. degree in electrical engineering, in 2014.

He has been with the Zhengzhou University of Light Industry, Zhengzhou, China, since 2014. His research interests include electromagnetic and thermalanalysis on electrical machine, especially in permanent magnetic machines.

ZHIHAO ZHU is currently pursuing the M.S. degree in electrical machines with the Zhengzhou University of Light Industry, Zhengzhou, China.

His current research interests include electromagnetic and thermal analysis on electrical machines, particularly on permanent magnetic machines.

BIN XIONG received the B.E. and M.E. degrees from the Harbin University of Science and Technology, Harbin, China, in 2002 and 2006, respectively, and the Ph.D. degree from the University of Chinese Academy of Sciences, in 2015.

He is currently an Associate Researcher with the University of Chinese Academy of Sciences. His research interests include motor system design, evaporative-cooling, and service behavior of electrical equipment.

CUNXIANG YANG received the graduate degree in electrical engineering from the Zhengzhou University of Light Industry, Zhengzhou, China, in 1988, and the Ph.D. degree in control science and engineering from the Huazhong University of Science and Technology, Wuhan, China, in 2009.

Since 1988, he has been with the Zhengzhou University of Light Industry. His research interests include intelligent control and electrical fault diagnosis technology.